Bachelor's Thesis Project

CO induced faceting of Rh(553)

Author: LAI Ka Sin
Supervisor: Johan Gustafson

Project Duration: 2 months

LUND UNIVERSITY

Department of Physics
Synchrotron Radiation Research
Spring Semester 2015

Abstract

We have investigated the CO induced faceting of a Rh(553) surface using Scanning Tunneling Microscope (STM), Low Energy Electron Diffraction (LEED) and Auger Electron Spectroscopy (AES). The sample was exposed to a CO pressure of 1×10^{-3} mbar, at different sample temperatures. The experiment was performed in the STM lab at the division of Synchrotron Radiation Research at Lund University. According to a recent surface X-ray diffraction study [1], the Rh(553) was reshaped into (110) and (111) facets, under CO rich reaction conditions for catalytic CO oxidation, in pressures of 0.1-300 mbar. In this project we tried to find if the faceting can also be found by exposure to pure CO at a lower pressure. The main result of the CO exposure, however, is a roughening of the surface. The roughening process is independent on the conditions we performed and the resulting surface consists of a significant amount of kinked steps and areas of various step size. Local areas of (110) surface is observed, but no systematic change of areas as found in ref. [1].

Contents

0.1 Abbreviations and Acronyms

STM	Scanning Tunneling Microscope
LEED	Low Energy Electron Diffraction
AES	Auger Electron Spectroscopy
UHV	Ultra-High Vacuum
LCAO	Linear Combination of Atomic Orbitals
CTRs	Crystal Truncation Rods

Chapter 1

Introduction

Catalysts are widely used in different areas and industries, since catalysis can help accelerating chemical reactions without itself being consumed. Using a catalyst can reduce the energy cost by forming bonds with the reactants, which opens up alternative reaction paths. The variation in the energy of the corresponding transition states affects the rate of the chemical reaction. One of the most common example is the oxidation of CO into CO_2 by using a metal catalyst like Rh, Pt or Pd. During the reaction, the oxygen molecules are adsorbed on the catalyst, and in this process they dissociate into oxygen atoms. A co-adsorbed CO molecule can then react with the oxygen atom and form CO_2. This kind of reaction is very useful as it can be used in cars to clean up the exhaust gases. Moreover, most chemical industries use catalysts in their production. Due to the increase of awareness of the environment, many studies on catalysis reaction are underway to gain more knowledge on the fundamental processes involved and the structure of the catalyst.

In a recent surface X-ray diffraction study, a stepped Rh(553) surface was investigated *in situ* while the CO oxidation reaction was running at pressures of about 0.1-300 mbar [1]. During catalytic CO oxidation under low pressure (0.1-1 mbar), it is found that under stoichiometric CO and O_2 conditions, the Rh(553) surface maintains its surface orientation without facet formation. In oxygen excess, the CO oxidation reaction becomes mass transfer limited by the diffusion of CO to the surface, and the surface is observed to expose (331) or $(11\bar{1})$ facets in coexistence with larger (111) terraces. Different facetings of Rh(553) are shown in Fig. 1.1. This finding is consistent with previous research on the exposure of Rh(553) to lower pressures of pure O_2 [2]. In CO excess condition, coexisting (110) and (111) facets are found on a CO poisoned surface with low activity. To summarize, the surface morphology changes dramatically depending on the mixture of reactant gases that the surface was exposed to. However, the structures found under CO rich conditions are previously not found.

In this project, the aim is to establish whether the faceting found during catalytic CO oxidation over Rh(553) under around 0.1 mbar and CO rich con-

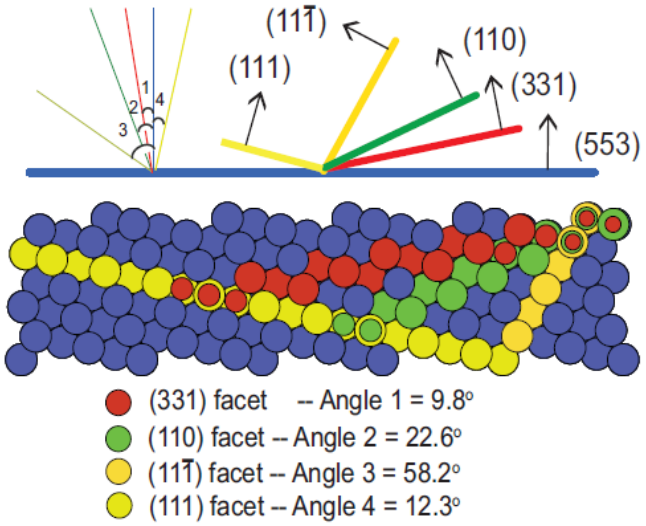

Figure 1.1: Model of the Rh(553) surface with different gas-induced facets

ditions can be seen in pure CO at lower pressures. That is, the investigation is to find out if the CO induced structure, similar to the oxygen induced one, can be formed in lower pressures of pure CO.

During the experiment, we used a combination of scanning tunneling microscopy (STM), low-energy electron diffraction (LEED) and Auger electron spectroscopy (AES).

1.1 Pressure conditions

In order to investigate the surface of the catalyst and prepare a well-defined surface, ultra-high vacuum (UHV) conditions (pressure lower than 10^{-9} mbar) is used. Under UHV conditions, the atomic arrangement of surfaces, surface reconstructions, and surface imperfections can be examined without the surface being contaminated too fast. Also, by carefully exposing the system to different reactant gases, not only the interaction between the surface (substrate) and the gas (adsorbate), but also adsorbate–adsorbate interactions can be studied. However, there is a difference between the idealized model under UHV conditions and industrial catalysts, which usually operates at atmospheric or higher pressures [3]. The difference is so called pressure gap. Recently, there are lots of papers studying the catalyst under pressure conditions ranging from UHV to realistic pressures [4, 5].

In the present project, a Rh(553) crystal was exposed to a CO pressure of about 1×10^{-3} mbar. The pressure in the chamber was controlled at 1.5×10^{-5} mbar, but the gas inlet was very close to the surface, such that the local pressure was about two orders of magnitude higher.

1.2 Material

Most of the common catalysts are based on transition metals. A transition metal is an element whose atom has a partially filled d sub-shell. Unlike s and p orbitals, d orbitals are more localized, and the band–width and energy level of the d-band will determine the metal's ability to form and break chemical bonds with different reactants. According to the tight binding theory, the electron states can be described by the linear combination of d-orbitals (LCAO) [6]. Therefore, the width of the d-band depends on the number of neighbour atoms. At the surface, the number of neighbour atoms is lower than in the bulk, and the d-band width is reduced. However, the number of electrons per atom in the d-band remains constant. The energy level of d-band should then increase if it is more than half-filled [7]. A higher energy d-band structure can bind more strongly to the gas like CO. In this case, this makes Rh a good metal for CO adsorption.

Similarly, defect sites, such as steps, kinks and vacancies, have even fewer neighbouring atoms, and hence narrower d-bands than the atoms on a flat surface. For Rh, this leads to an even higher energy of the d-band and the corresponding atoms can bind more strongly to the gas molecules. All in all, these under-coordinated atoms on the surface can enhance the adsorption energy of the adsorbates and even promote the dissociation of them and lower the activation energy for certain reactions. Industrial catalysts usually consist of metal nanoparticles, which expose many under-coordinated atoms. The activity of a catalyst depends strongly on the microscopic details of the nanoparticle like its shape, adsorption behaviour on different facets or defect sites and adhesion to the oxide substrate.

One way to increase the complexity of the surface, in order to study the effect of such under-coordinated atoms, is to use stepped or vicinal surfaces. By studying the step dynamics of this kind of surface, fundamental information of complex catalysts can be found. Moreover, the use of the stepped surface model gives higher control of the surface chemistry and structure than the real catalyst. It can enhance the understanding and be used for an improvement of industrial catalysts. Over the past decades, lots of the studies have been done, investigating vicinal metal surfaces, see for instance ref. [8]. Recent research shows the atomistic mechanisms governing oxygen-induced morphology changes of a vicinal Rh(553) surface [2]. It implies that the important properties of a catalytic nanoparticle may be transformed when it is exposed to a particular gas pressure and/or temperature. Research on Rh(553) can lead to understanding the property of heterogeneous catalysis, such as the atomic geometry and composition of the catalyst.

Although there are differences between this model system and industrial systems with respect to pressure (pressure gap) and complexity (material gap), understanding of the basic behaviour and the process of catalysts can still be found, which is crucial to the improvement of catalysts.

Chapter 2

Experimental setup

2.1 Sample: Rh(553) surface

The orientation of a surface or a crystallographic plane is usually described by the so called Miller Indices. The Miller indices (hkl) are defined such that a vector (h, k, l) is perpendicular to the corresponding plane. This plane also intersects the crystallographic axes of the solid in $(\frac{1}{h}, \frac{1}{k}, \frac{1}{l})$.

Low index surfaces refers to the Miller indices being small numbers (0 or 1), e.g. (100), (110) and (111). These surfaces are flat, without any steps or kinks. High index surfaces refer to one or more of the Miller indices being higher than 1. Such a surface can be obtained by cutting a single crystal with a small angle to (or in the vicinity of) a low index plane. Hence, these are also referred to as vicinal surfaces. Rh(553) is one of the vicinal surfaces, which is cut with an angle of 12.3° relative to the (111) plane. The result is five-atom-wide (111) terraces separated by monoatomic $(11\bar{1})$-faceted steps. The model is shown in the Fig. 2.1.

2.2 Scanning Tunneling Microscope

The Scanning Tunneling Microscope (STM) was developed by Binning and Rohrer [9]. It can depict a solid surface with atomic resolution, such that individual atoms can be imaged and manipulated. STM can be used not only in UHV condition but also in various liquid or gas ambience, and the the working temperature range can be from few K to about 1000 K.[10]

2.2.1 Working principle

Tunneling is a quantum mechanical effect in which electrons penetrate through a classically impenetrable potential barrier. In STM, the electrons tunnel from the surface through the vacuum barrier to reach a probing tip or vice versa. It can be explained from quantum physics that the wave function of the electron

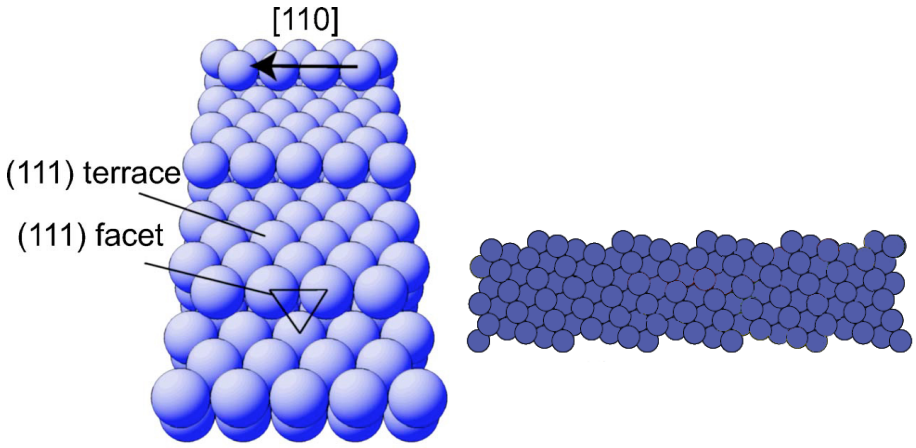

(a) (b)

Figure 2.1: (a) Model of the Rh(553) surface, adapted from [2]; (b) Sideview of Rh(553);

does not drop to zero exactly at the barrier, instead it extends a little into the vacuum region. This leaking of the function allows electrons to pass the classically forbidden regions.

The basic tunnelling effect is shown in Fig. 2.2. The two electrodes are separated by a vacuum barrier, with the left and right electrodes representing the tip and sample, respectively. Each electrode has an associated potential and eigenstates that satisfy the Schrödinger equation within that electrode, e.g:

$$i\hbar\frac{\partial\Psi}{\partial t} = [-\frac{\hbar^2}{2m}\frac{\partial^2}{\partial z^2} + U_s]\Psi$$

with

$$\Psi = \psi_s e^{-iE_s t/\hbar}$$

and

$$[-\frac{\hbar^2}{2m}\frac{\partial^2}{\partial z^2} + U_s]\psi_s = E_s\psi_s$$

where ψ_s is the stationary state with Eigenvalue E_s.

For each electrode, the wavefunctions of these eigenstates decay into the vacuum. However, if the vacuum region is small enough, there is still some probability that an electron on one electrode will hop onto the other electrode. It can be seen in the Fig. 2.2 that there is overlap of two wavefunctions in the vacuum region.

By setting a bias voltage between the measuring tip and the sample (Fig. 2.3), a tunnel current is induced. This current depends exponentially on the distance d between the tip and the sample surface. The equation is approximated as [12],

$$I_T \propto \frac{U}{d}e^{(-Kd\sqrt{\bar{\phi}})}$$

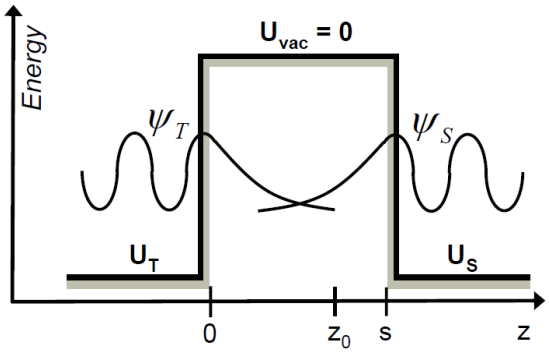

Figure 2.2: Schematic of a planar tunnel junction between two electrodes with zero bias between them. The wavefunctions on each electrode decay into the vacuum region between them, where T for tip and S for sample. Adapted from [11]

where I_T is the tunnel current, U is the bias voltage, $\bar{\phi}$ is the average work function of the tip and sample, and K is a constant. The work function is the energy needed to remove an electron from the material to the vacuum level.

By scanning the tip over the surface, at constant height, and monitoring the tunnel current as a function of position at the surface, an image of the surface is created. Alternatively, the height of the tip can be adjusted in order to keep the current constant. The variation of the normal position of the tip is then plotted and translated to the topology of the surface. These two modes of running the STM are referred to as the constant height mode and constant current mode, respectively. Which mode to use depends on the properties of the sample. In this experiment, the constant current mode is used.

After analysing the data, a picture of the electronic states at the surface is actually measured, but to a first approximation, this can be interpreted as the topography of the surface.

2.2.2 Instrumentation

As the imaging of the surface is of atomic scale, the movement of the tip across the surface must be controlled on an Å level. This is the hardest part in the experimental setup. A typical setup of STM is shown in Fig. 2.4.

First of all, the sample is mounted on a support which can be driven by an extremely small current change. The legs which are attached to the metallic support plate act as clamps to hold the sample by applying a voltage. The scanning of the tip across the surface is performed by means of the piezoelectric triple legs. The piezoelectric effect is the linear electromechanical interaction between the mechanical and the electrical state in crystalline materials due to the electric dipole moments in it. The piezoelectric triple legs change dimensions in response to an applied voltage, and hence control the tip position in x, y and

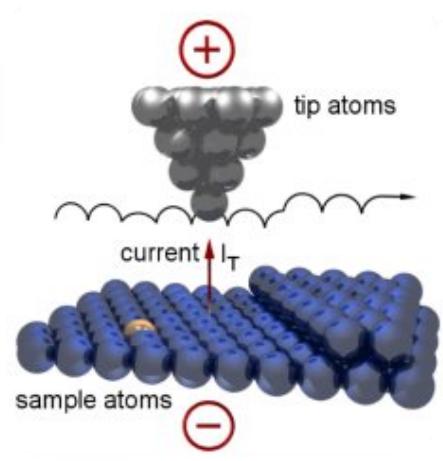

Figure 2.3: Keeping the tunnelling current constant while scanning the tip over the surface, the tip height follows a contour of constant local density of states. Adapted from [13]

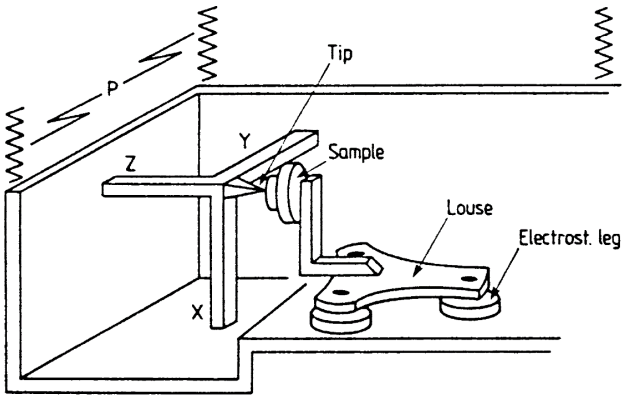

Figure 2.4: Schematic of a typical STM, adapted from [9]

z directions. An accuracy better than 1 Å is obtained by biasing the piezodrive by a few tenths of a volt.

In this project, an Omicron STM1 was used, which has a similar design as shown in Fig. 2.4

The difficulties of STM include the suppression of mechanical vibrations of the setup and the preparation of the tip. The vibration can be damped by suspending the setup on a very soft springs. The tip is prepared from W wire. In this experiment, the tip was sputtered with Ar gas and crashed on a Ag surface to remove oxides on the tip.

2.2.3 STM of Rh(553)

Fig. 2.5 shows STM images of the clean Rh(553) surface, where steps can be seen clearly in each image. The step edges are not very straight and the terrace width also shows some variation. However, the average distance between steps is around 1.09 nm (see Fig. 2.6), which is close to the theoretical value of 1.03 nm. The STM can also be compared with the one in a previous study [2], which shows a similar structure and also similar measured step size.

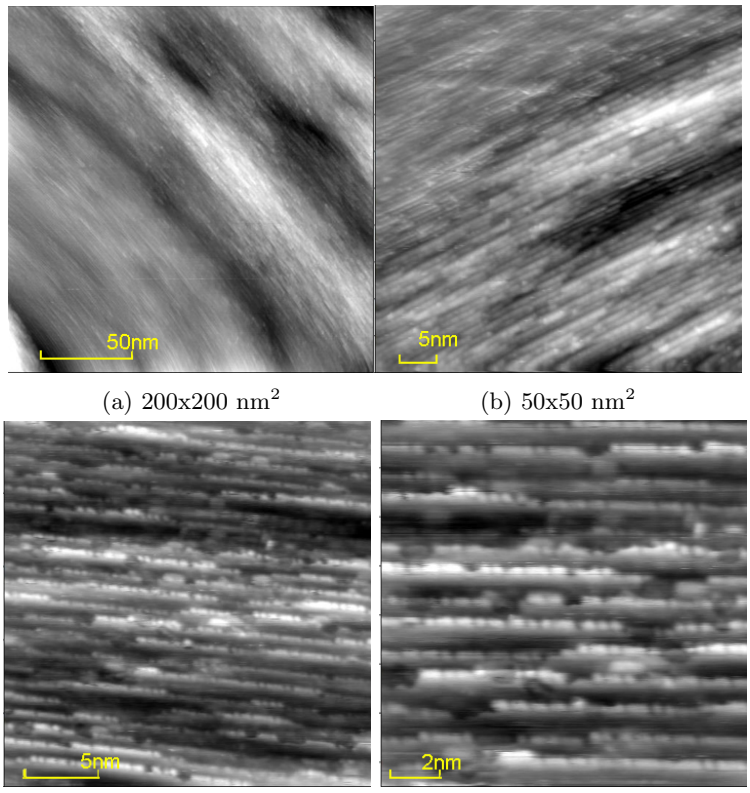

(a) 200x200 nm^2 (b) 50x50 nm^2

(c) 25x25 nm^2 (d) 15x15 nm^2

Figure 2.5: STM image of clean Rh(553)surface

2.3 Low Energy Electron Diffraction

LEED is a method that makes use of the wave nature of electrons to understand the structure of the solid surface. The surface structure of single-crystalline materials can be determined by bombardment with a collimated beam of low energy electrons and observation of the resulting diffraction pattern of backscattered electron. It can identify the surface structure of the sample by comparing the

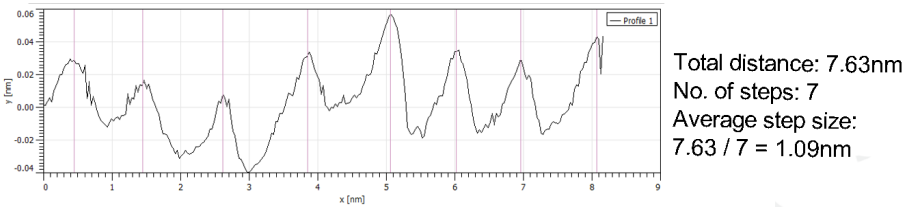

Figure 2.6: The step size measured is around 1.09 nm, which is close to the calculated step size of Rh(553) of 1.03 nm

result with the LEED patterns of the known samples or theoretically calculated patterns.

2.3.1 Working principle

Consider two atoms separated by a vector **R**, as shown in Fig. 2.7a, and an incoming plane wave with wave vector **k** that is scattered elastically by the two atoms forming diffracted wave with wave vector **k′**.

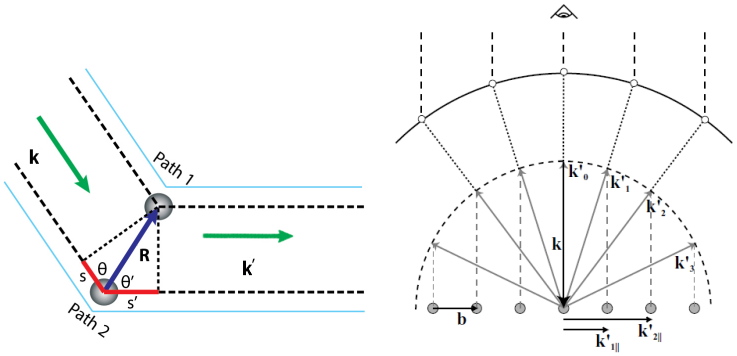

(a) (b)

Figure 2.7: (a) Constructive interference occurs if the path difference (s+s') is equal to an integer multiple of the wavelength. (b) In the LEED experiment, the reciprocal lattice vector $\mathbf{k}'_{\parallel}$ satisfies the condition $\mathbf{R}\cdot\mathbf{k}'_{\parallel} = 2n\pi$, where the constructive interference will be obtained

Under constructive interference, the path difference $(s+s')$ can be expressed as follow:

$$s + s' = R\cos\theta + R\cos\theta' = n\lambda$$

By using the scalar product(e.g. $\mathbf{R}\cdot\mathbf{k} = Rk\cos\varphi$, where $\varphi = 180°-\theta$ in Fig. 2.7a), the equation becomes:

$$s + s' = \mathbf{R}\cdot\left(\frac{\mathbf{k}}{|\mathbf{k}'|} - \frac{\mathbf{k}}{|\mathbf{k}'|}\right) = \mathbf{R}\cdot\frac{(\mathbf{k}'-\mathbf{k})}{k} = n\lambda$$

$|\mathbf{k}| = |\mathbf{k}'|$ because of elastic scattering.

By using the definition of the wave vector, $k = \frac{2\pi}{\lambda}$

$$\mathbf{R}\cdot(\mathbf{k}' - \mathbf{k}) = \mathbf{R}\cdot\mathbf{K} = 2n\pi$$

where $\mathbf{k} - \mathbf{k}' = \mathbf{K}$ and n is an integer.

Here we define $\mathbf{R} = n_1\mathbf{a_1} + n_2\mathbf{a_2} + n_3\mathbf{a_3}$, where $\{\mathbf{a_1}, \mathbf{a_2}, \mathbf{a_3}\}$ is a set of primitive vectors for the direct lattice in real space. Every vector $\mathbf{R}$ represents the position where an atom is sitting. For full constructive interference, the equation above should be fulfilled for all possible lattice vectors $\mathbf{R}$. The reciprocal lattice is now generated by the three primitive vectors:

$$\mathbf{b_1} = 2\pi\frac{\mathbf{a_2}\times\mathbf{a_3}}{\mathbf{a_1}\cdot(\mathbf{a_2}\times\mathbf{a_3})}, \mathbf{b_2} = 2\pi\frac{\mathbf{a_3}\times\mathbf{a_1}}{\mathbf{a_1}\cdot(\mathbf{a_2}\times\mathbf{a_3})}, \mathbf{b_3} = 2\pi\frac{\mathbf{a_1}\times\mathbf{a_2}}{\mathbf{a_1}\cdot(\mathbf{a_2}\times\mathbf{a_3})}$$

So, we have

$$\mathbf{b_i}\cdot\mathbf{a_j} = 2\pi\delta_{ij}$$

where δ_{ij} is the Kronecker delta function. Now, if we take $\mathbf{K}$ to be a linear combination of the $\mathbf{b_i}$, then,

$$\mathbf{K} = k_1\mathbf{b_1} + k_2\mathbf{b_2} + k_3\mathbf{b_3}$$

It forms a reciprocal lattice vector which satisfies the condition $\mathbf{R}\cdot\mathbf{K} = 2n\pi$, if k_i are integers.

Since the electrons interact strongly with matter, the diffraction can, to a first approximation, be considered originating from the top layer only. This means we only need to consider surface scattering, and the requirement for constructive interference can be expressed as

$$\mathbf{R}\cdot\mathbf{K}_{\parallel} = 2n\pi$$

Fig. 2.7b shows a schematic image of LEED, with a wave vector $\mathbf{k}$ coming in perpendicular to the reciprocal surface lattice, and scattered waves $\mathbf{k_i'}$ going out of the surface. The reciprocal surface lattice (with basis vector $\mathbf{b}$ in the figure) satisfies the condition of surface scattering stated above. Thus, the directions of the outgoing wave vectors must be such that their projections on the lattice reaches from one reciprocal lattice point to another. The screen is observed from the top, and a picture of the reciprocal lattice scaled into real space units can be observed [14].

An example of transforming from a real hexagonal Rh(111) lattice to its corresponding reciprocal lattice is shown in Fig. 2.8. In the figure, we have the real lattice defined by $\mathbf{a_i}$, the reciprocal lattice defined by $\mathbf{a_i^*}$. We can see that $|\mathbf{a_1}| = |\mathbf{a_2}|$,so $|\mathbf{a_1^*}|$ is also equal to $|\mathbf{a_2^*}|$, while the angle between $\mathbf{a_1^*}$ and $\mathbf{a_2^*}$ becomes 120°. Hence, the (111) terraces of our sample are expected to yield a LEED pattern similar to Fig. 2.8b.

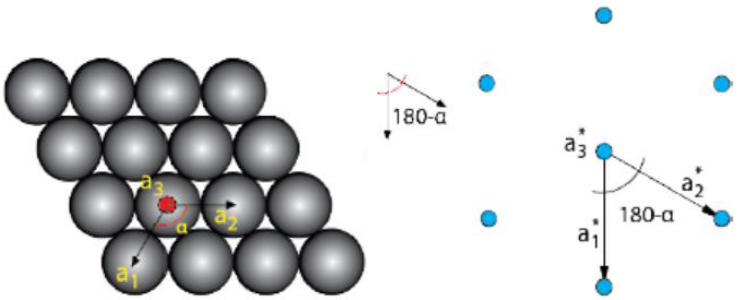

(a) (b)

Figure 2.8: (a) Hexagonal surface structure with the primitive unit cell vectors indicated as $\mathbf{a_1}$ and $\mathbf{a_2}$. $\mathbf{a_3}$ is a unit vector pointing out of the paper. (b) The reciprocal unit vectors $\mathbf{a_1^*}, \mathbf{a_2^*}, \mathbf{a_3^*}$ constructed from (a).

For the stepped surface, the periodically distanced steps act as a diffraction grating with the well-known equation

$$d \sin \varphi = m\lambda$$

where d becomes the step size in this case.

Therefore, in the LEED of Rh(553) surface, there is a splitting of the (111) dots due to the step periodicity. If there is faceting of the surface, e.g. if (110) facets are formed, then the splitting will be larger because of the smaller step size of (110) surface. In case of no faceting but just more disordered of the surface, the LEED pattern will become fuzzy and the dots will be indiscernible. The reason is that the intensity maxima of the diffraction depends on the order of the surface. The more disordered of the surface, the more diffuse background of LEED will be produced.

2.3.2 Instrumentation

The standard experimental set up for LEED consists of an electron gun to produce an electron beam with primary energies in the range of 20-500 eV and a display system for observing the diffraction pattern. This energy range is well suited to surface studies since the electrons have a short mean-free path in the solid and only penetrate a few atomic layers into the surface. This makes LEED (and other methods based on low energy electrons) very surface sensitive.

A typical three-grid LEED system is shown in Fig. 2.9. The electron gun unit consists of a heated filament with a Wehnelt cylinder W followed by an electrostatic lens system A, B, C, D. The acceleration energy (20-500 eV) is set by the potential between the cathode and apertures A and D. Apertures B and C are used to focus the electron beam. Generally, the apertures in the electron gun unit and the grids in front of the fluorescent screen are used to collimate the beam to prevent aberration of the image. Aperture A and D, as well as, the

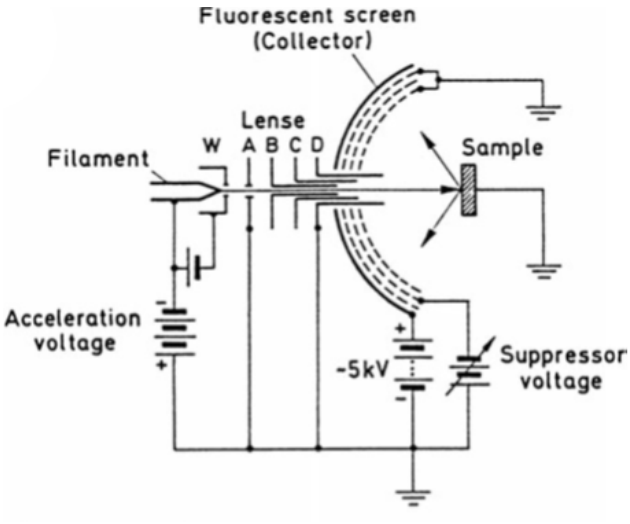

Figure 2.9: Schematic of LEED optic, adapted from [6]

first and the last grid before the fluorescent screen, are grounded. As a result, a field-free space is established between the sample and the display system through which the electrons travel to the surface and back after scattering.

By giving the middle grid a negative bias, the inelastically scattered electrons cannot pass through. The illumination given by the inelastically scattered electrons can therefore be suppressed. Finally, the fluorescent screen (collector) has to be at positive potential (e.g. 5kV in Fig. 2.9) in order to achieve a final acceleration of the slow electrons; only high-energy (elastically scattered) electrons can be made visible on the screen.

2.3.3 LEED of Rh(553)

In the experiment, the clean Rh(553) surface is first checked before any CO dosing process is carried out. Fig. 2.10 shows the LEED measurements with 3 different beam energies. The diffraction pattern confirms the presence of a well-ordered Rh(553) surface, with the expected hexagonal pattern of split dots.

2.4 Auger Electron Spectroscopy

Auger Electron Spectroscopy (AES) is an analysis technique to study which elements are present on the surface. It is used mainly to check the cleanliness of a freshly prepared surface under the UHV conditions, but it can also be used to study film growth, surface-chemical composition and depth profiling of the concentration of particular chemical elements. By observing peaks at specific energy values, the material of the sample and also the impurities on the surface

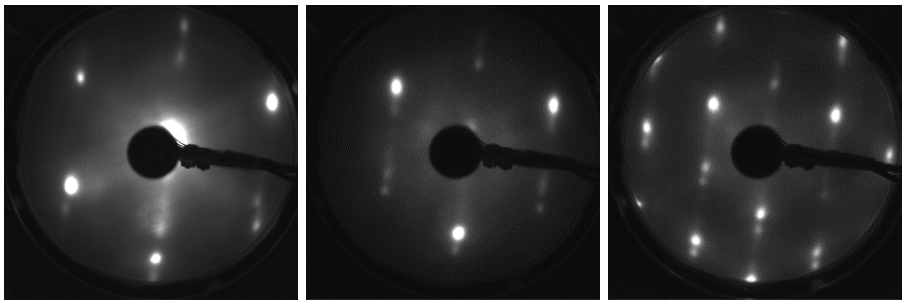

(a) 60eV (b) 90eV (c) 150eV

Figure 2.10: LEED of clean Rh(553) surface.

can be identified.

2.4.1 Working principle

In AES, a primary electron beam is excited from an electron gun. The beam ionizes an atom in the sample and produces a hole in a core electron level (K or L shells). This hole is filled by an electron originating from an energetically higher-lying shell (e.g. M shells or valence bands in solids). The energy gained by the electron that transfers into the deeper atomic level, is transferred to another electron of the same or a different shell, which is in turn emitted from the sample. This transition is called Auger transition and the electron emitted is called Auger electron. The kinetic energy of the Auger electron is directly related to differences in electron energies, and by measuring this energy, particular elements can be identified in the sample. A schematic picture of the Auger process is displayed in Fig. 2.11. In this example, the incoming electron beam knocks out a electron in the core electron level, which is indicated by the broken arrow. An electron hole is then created in the L_3 shell. The hole is filled by an electron from the valence band and the energy is transferred to a third electron, which leaves as an Auger electron. This is indicated by the solid arrow.

2.4.2 Instrumentation

The equipment for AES consists an electron gun that provide an electron beam with energy from 2000 to 5000eV. The typical energy analysers are hemispherical or cylindrical mirror analysers, which use varying electric fields to sort out and detect electrons of different energies. The AES raw data is usually derivated during analysis in order to suppress the large background of secondary electrons.

A schematic picture of a standard experimental setup for AES is shown in Fig. 2.12. In this graph, as in out experiments, a Cylindrical Mirror Analyser is used.

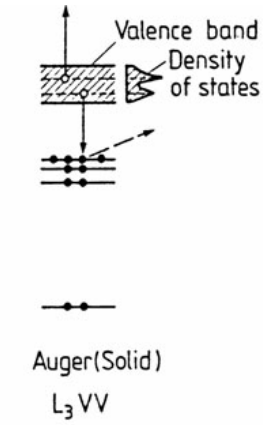

Figure 2.11: Auger process in solid, adapted from [15]

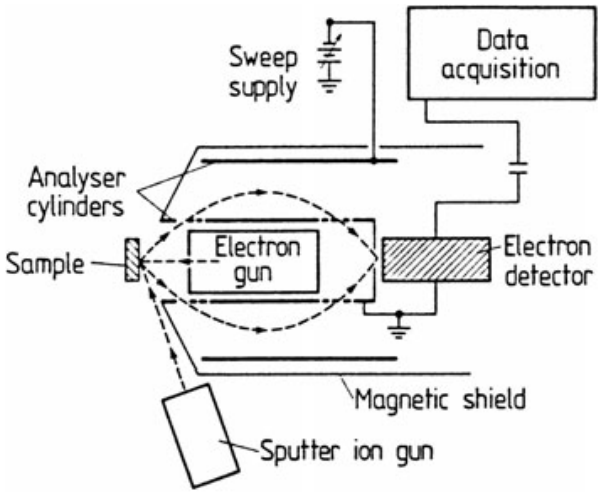

Figure 2.12: Schematic picture of an AES setup using a cylindrical mirror analyser, adapted from [16]

2.4.3 AES of Rh(553)

Fig. 2.13 shows AES data from the clean Rh(553) crystal. Peaks corresponding to Rh and C would appear at about 299 eV and 272 eV, respectively, which is within the range plotted in Fig. 2.13a. Here we do find a peak corresponding to Rh, but not to C, as expected for the clean surface. In Fig. 2.13b, where we would expect a peak corresponding to O, we find a straight line with no peak around 503 eV. It is then concluded that the surface is relatively clean, without any C and O impurities. For all AES measurements in the experiment,

the measured energy is actually about 3 eV smaller than expected, due to an instrumental calibration error. Moreover, the peak corresponding to O (which will be shown below) is so weak that the raw data is plotted directly, without differentiation.

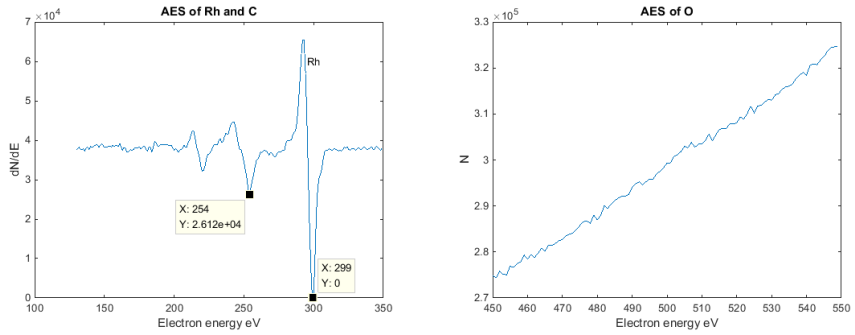

Figure 2.13: AES of clean surface

2.5 Experiment procedure

Firstly, the chambers were baked (heated) for 48 hours in order to remove impurities (mainly water molecules) from the walls of the chamber, and hence be able to reach UHV pressures. Then the sample was put into the preparation chamber. A process of sputtering with Ar^+ and annealing at 900°C was repeated several times to clean and remove impurities on the sample. It was followed by exposure to oxygen gas at 1x10^{-6} mbar while varying the temperature between 300°C and 700°C to remove carbon on the surface. After exposure of O_2, annealing was needed to desorb the oxygen from the surface and to make the surface smooth again. The process of oxygen exposure was also repeated for several times. The sample was then transferred to analysis chamber to undergo AES, LEED and STM measurements in order to confirm whether a clean Rh(553) surface is obtained. Apart from the cleaning of the sample, the sputtering of the tip of the STM was also performed, as the tip appeared to be of quite low quality.

For the CO dosing, the gas inlet was moved very close to the surface, so that the local pressure can reach around 10^{-3} mbar although the pressure in the chamber was controlled at 1.5x10^{-5} mbar. Different temperatures of the sample and different dosing times were applied. Then the sample was checked for differences in LEED pattern, and if there are any carbon and oxygen peaks in AES. Any changes of the surface structure were observed by STM.

The oxygen treatment and annealing process were repeated between each experiment in order to assure a clean sample surface before dosing CO.

During the experiment, different conditions had been set up in order to find out if they caused any differences in the sample structure. The CO dosing conditions are as follow (The CO gas is turned off after the sample is cooled down, if not stated): 250°C under 5 minutes, 250°C under 5 minutes with the CO gas turning off before the cooling of the sample, 250°C under 15 minutes, 350°C under 5 minutes, and room temperature under 5 minutes. The pressure in the chamber was set to $1.5\text{x}10^{-5}$ mbar in all conditions.

Chapter 3

Result and Discussion

We have exposed the Rh(553) surface to CO under five different conditions, as summarized in Table 3.1. The LEED, AES and STM of the sample for different conditions are discussed below.

Temperature (°C)	Dosing Time (min)	Pressure (mbar)	Comment
250	5	10^{-3}	Cool down in CO.
250	5	10^{-3}	Cool down in vacuum.
250	15	10^{-3}	Cool down in CO.
350	5	10^{-3}	Cool down in CO.
room temperature	5	10^{-3}	Cool down in CO.

Table 3.1: Table of different dosing conditions

3.1 LEED

LEED of the different sample preparations are shown in Fig. 3.1. It is found that the spots in all pictures are not as sharp and bright after CO exposure as for the clean surface. For the condition where the CO was turned off before cooling (Fig. 3.1b), the LEED shows even more changes, with a big but fuzzy and bright area observed at the center of the screen. We cannot deduced what kind of surface structure this corresponds to. However, the surface is certainly more disordered compared with the previous condition where the heat was turned off first. When the gas is turned off first, the CO is expected to leave the surface but the temperature is not high enough in order to get back the well ordered (553) surface. For the condition of 250°C and 15 mins (Fig. 3.1c), the LEED shows a little more fuzzy pattern compared to the one with 5 mins (Fig. 3.1a) as the splitting of the dots is less observable. This suggests that it is more disordered of the surface structure. This result is quite straight forward to explain, as the time of reaction increases, the CO molecules have more chances

and time to adsorb and rearrange the surface. The LEED pattern is then more likely to be disturbed. For the exposure at room temperature, it can be seen that the hexagonal pattern in the LEED is the obscurest. Most of the dots are very dim and some cannot even be observed. This indicates that even at room temperature the surface atoms are mobile enough to be rearranged by CO.

Overall, the LEED shows more diffused pattern of Rh(553) for all CO exposures, but there is no obvious larger splitting of the spots. This means that we cannot find any systematic changes of the surface where (110) facets are formed. However, CO is still found to be adsorbed on the surface, and the surface becomes more rough in all cases.

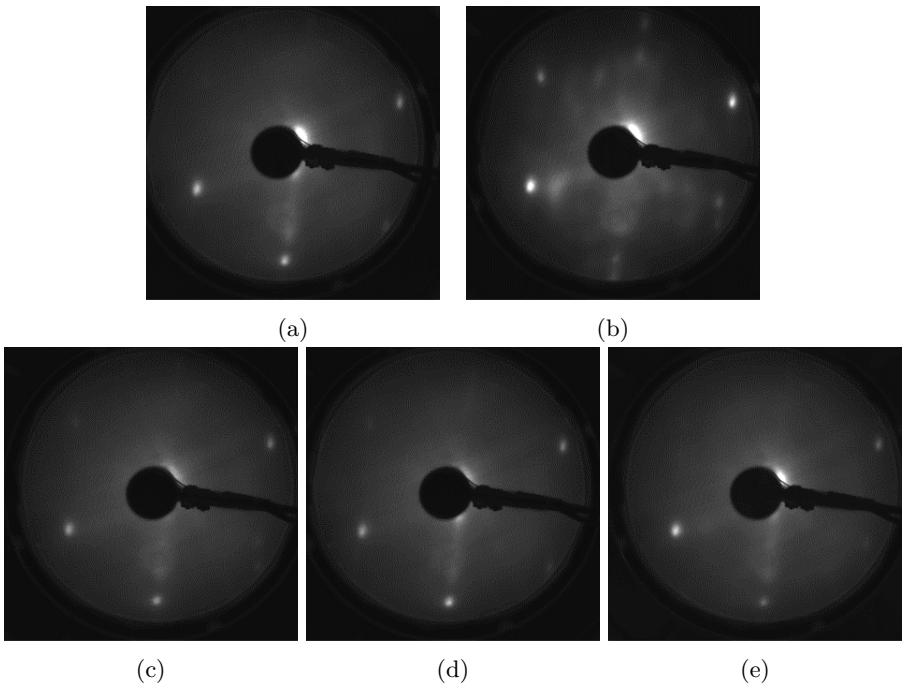

Figure 3.1: LEED under different conditions (60eV): (a) 250°C, 5 mins; (b) 250°C, 5 mins (with CO gas off first); (c) 250°C, 15 mins; (d) 350°C, 5 mins; (e) room temperature, 5 mins

3.2 AES

Fig. 3.2 shows the AES of O for different dosing conditions. For all conditions where the sample was cooled before the CO exposure stopped, we find a peak around 503eV, which is where the characteristic peak of O is expected. This confirms that there is CO on the surface. However, for the condition where the CO exposure was turned off first, the peak around 503eV is absent, which

confirms that the CO desorbs from the surface when the exposure stops at 250°C. For the longer exposure of 15 minutes at 250°C, the peak is stronger as compared to the shorter exposure at the same temperature, but the strongest peak is found for the exposure at 350°C. A rougher surface will have a larger surface area, and hence be able to accommodate more CO. We then interpret these results as the 15 min exposure resulting in a rougher surface, since there is more time for the process, and the higher temperature gives an even rougher surface since the atoms are more mobile and the surface is easier to make rough. This also agrees with the relatively low AES signal from the room temperature exposure.

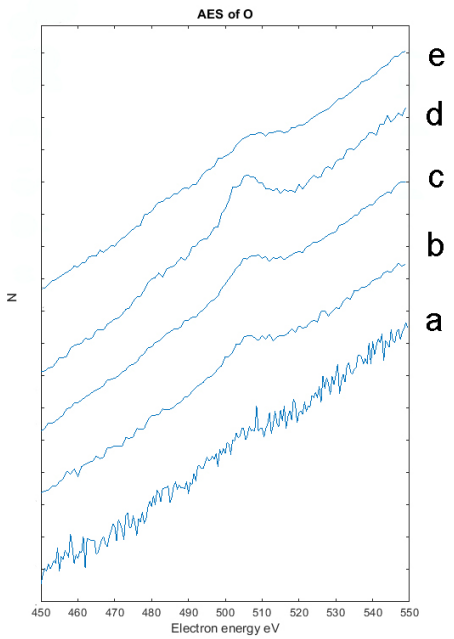

Figure 3.2: AES under different conditions: (a) 250°C, 5 mins (with CO gas off first); (b) 250°C, 5 mins; (c) 250°C, 15 mins; (d) 350°C, 5 mins; (e) room temperature, 5 mins

3.3 STM

In general, the roughness of the surface increases in all conditions, and no huge differences were found between different conditions. Against our expectations, we did not find any systematic faceting of the surface, into (110) and (111) oriented areas. Fig. 3.3 shows the STM of some of the conditions. It is easy to observe that the step size varies a lot and also a triangular form of steps can be found. The step size is also measured for the condition 250°C, 5 mins with CO

gas off first and the condition under room temperature, 5 mins, they are shown in Fig. 3.4. They are found to be varied from the original step size of clean Rh(553) which is 1.03 nm (Fig. 2.6) but still there is no systematic change of step size and it doesn't fit the step size corresponding to (110) or (111) surfaces also. The surface is just mainly getting more rough by forming areas of different step sizes.

Moreover, referring to a recent paper [17] on the investigation of exposure of CO on stepped platinum surface. The STM images of their result revealed a doubling of terrace width and step height on the Pt(557) surface. We cannot find this change of the surface structure, as the average step size we found doesn't deviate significantly from the original step size, as mentioned above.

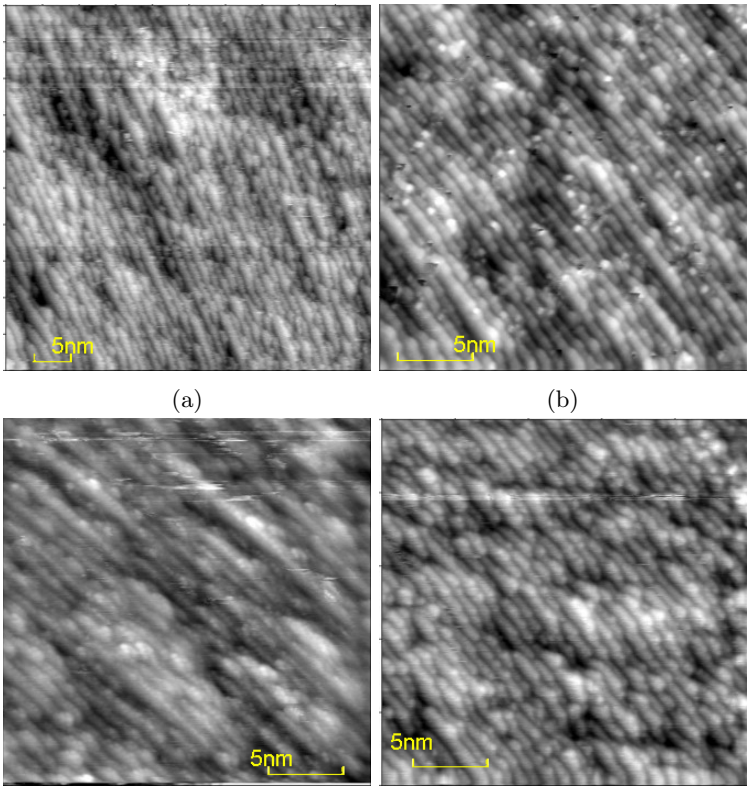

Figure 3.3: STM images of some conditions: (a) 250°C, 5 mins (50x50 nm^2); (b) 250°C, 5 mins with CO gas off first (25x25 nm^2); (c) room temperature, 5 mins (25x25 nm^2); (d) 250°C, 15 mins (25x25 nm^2); It can be seen that all surfaces are roughened compared to the STM of clean surface stated above.

While the surface becomes more rough, kinks are found in the steps. Kinks are formed by the relocation of the step edge atoms due to the adsorption of

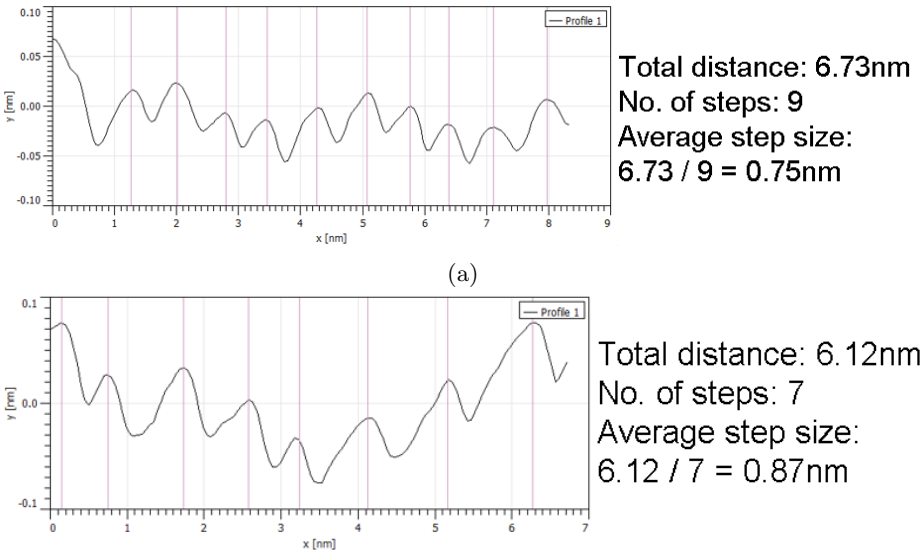

Figure 3.4: Step size is calculated for some of the conditions: (a) For 250°C, 5 mins with CO gas off first, the step size is around 0.75 nm; (b) For room temperature, 5 mins, the step size is around 0.87 nm. It shows that there is neither faceting nor the doubling of the step size.

CO. An illustration and an atomic model of kinks are shown in Fig. 3.5. Fig. 3.6 shows kinks formed for the condition of 350°C with 5 mins. In the paper referred to above [17], they observed a large area of uniform triangular structure, which they deduced was formed because this kind of structure is energetically more favourable. In our case, either the energetics are different due to the different surface materials or the exposure time is not enough to rearrange the surface into a new well ordered structure. The relocation of the edge atoms to form the kinks needs energy but if the energy released for CO adsorb on the kink site can compensate it then the kink formation is still energetically favourable. As the total energy of the surface is lower, the surface can become more stable through this kink formation process.

According to the STM image in Fig. 3.6b, at least 7 atoms can be found in one of the widest steps. The average step size is also measured to around 1.2 nm (Fig. 3.7). When some steps form relatively wide terraces, there should be some areas with smaller terraces in order to compensate the total area. Fig. 3.8 shows such an area with (110) like structure. By measuring the ratio between long axis and short axis of the unit cell in STM, it is found to be 1.42, which is consistent to the theoretical ratio of $\sqrt{2} = 1.414$ for the (110) unit cell. The model of the (110) unit cell and the determination of the theoretical ratio between long and short axis of the unit cell are illustrated in Fig. 3.9. Although this (110) facet is

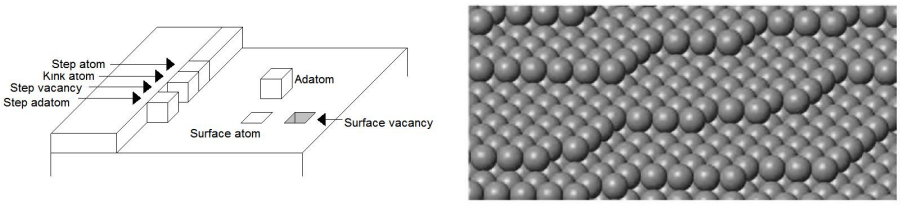

(a) (b) Atomic model of kinks, adopted by [18]

Figure 3.5: (a) Definition of the kink, which it is formed by relocating the edge atoms; (b) Kinks in an atomic model

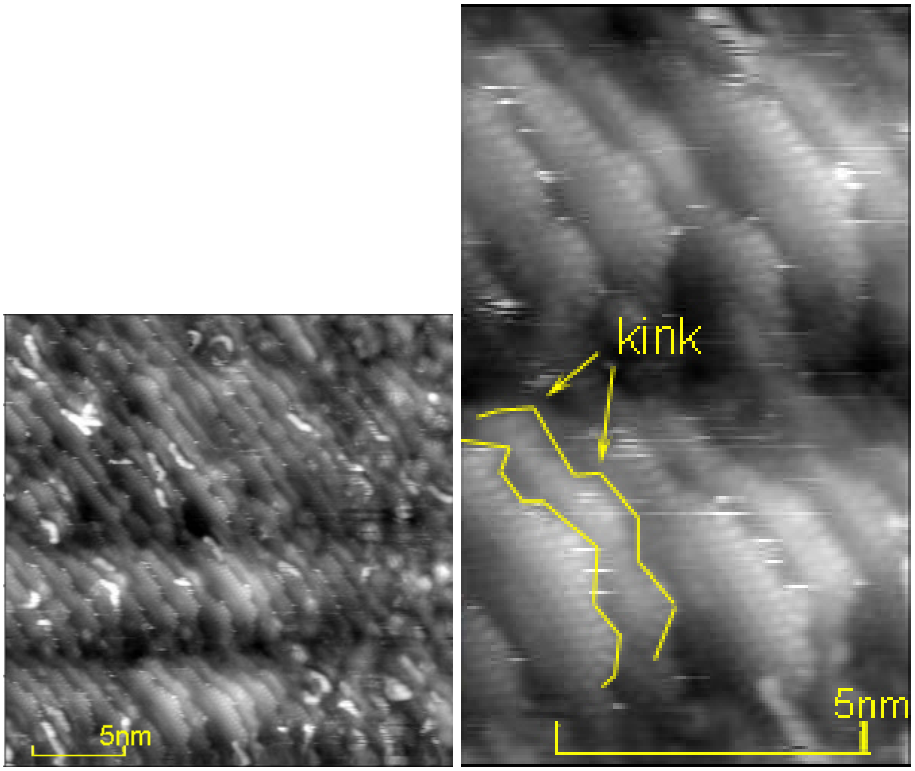

(a) 25x25 nm^2 (b) Zoom in image from Fig. 3.6a

Figure 3.6: STM under condition of 350°C, 5 mins: the surface is roughened by forming lots of kinks under the adsorption of CO molecules.

found, it only happens locally on a small area. All in all, no systematic faceting is found. The surface just becomes very rough with patches of large and small step sizes.

The reason for not finding the large (110) facets is probably that the CO pressure need to be in the range around 0.1 mbar in order to make these facets energetically favourable, as discussed briefly in ref. [1].

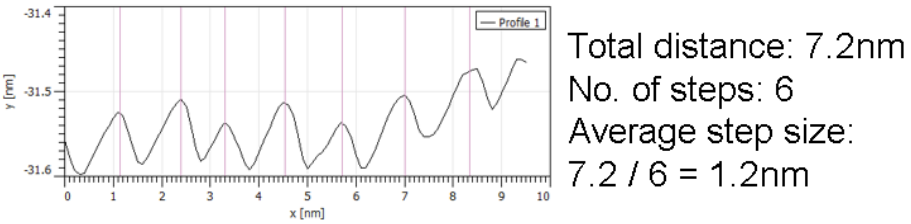

Figure 3.7: The step size calculated is around 1.2 nm in the wide step area for the condition 350°C, 5mins. It is considerably larger than the original step size of Rh(553).

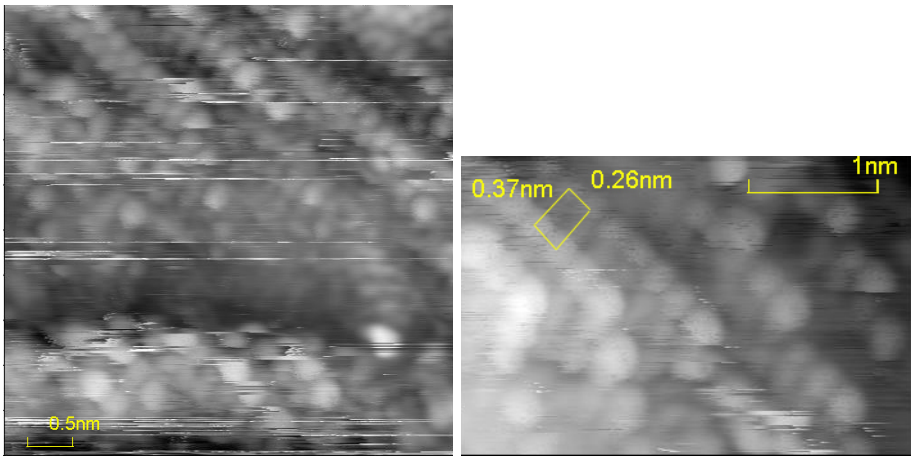

(a) 5x5 nm^2 (b) Zoom in image from 3.8a

Figure 3.8: (110) like structure is found under condition of 350°C with 5mins, the length of long and short axis of the unit cell is found in (b), the ratio is calculated to be about 1.42, which is very close to the ratio of unit cell of (110) which is $\sqrt{2} = 1.414$..

According to our results, the roughening of the surface does not depend significantly on the temperature. Even at room temperature the atoms on the surface have sufficient energy to relocate themselves when exposed to CO. Comparing the preparations where the exposure to CO was stopped before or after the sample was cooled, it shows that the rearranged surface doesn't transform back even the CO gas is desorbed.

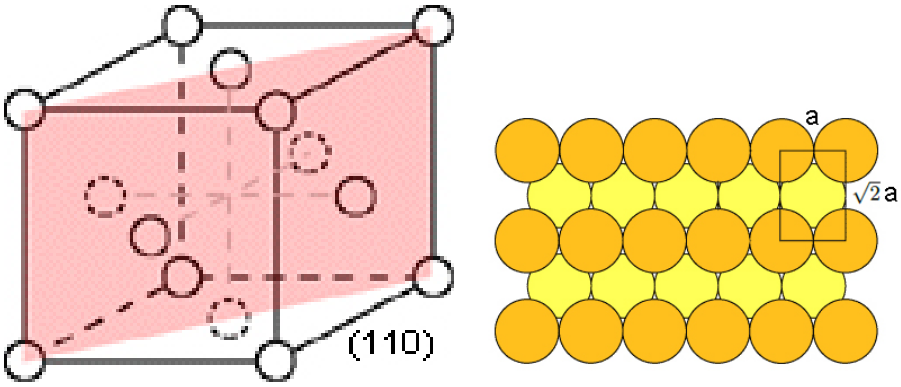

(a) (b)

Figure 3.9: (a) (110) face from the unit cell; (b) the theoretical ratio between the long and short axes of the unit cell is $\sqrt{2}$

Chapter 4

Conclusion

In conclusion, we have investigated the CO-induced faceting of a Rh(553) surface under different CO dosing conditions. We find that the surface becomes very rough with varying step sizes under all conditions but (110) faceting cannot be found in general. The step structure is rearranged by forming kinks. The formation of kinks is thought to be lowering the total energy of the surface, and thus the CO covered surface is stabilized. Although a large (110) facet is not found, areas of different step sizes are observed. While areas of larger step sizes are formed, there should be other areas where the step size has shrunk in order to maintain the total number of steps. A small area of (110) surface is found, as confirmed by measuring the ratio of long and short axes of the unit cell. The reason for not finding (110) faceting with large (111) terrace, which is observed in previous study [1], may be the low pressure of CO. In the previous study, 0.1-300 mbar was used while we only use $1x10^{-3}$ mbar of CO gas in this experiment.

Similar results are observed under all conditions, which means that the roughening doesn't depend much on the conditions we have varied. Even under room temperature, the surface atoms have enough energy to relocate themselves. Moreover, the desorption of CO molecules doesn't affect the roughened surface; it seems like CO molecules cause the roughening during the adsorption process and it is not necessary for them to stay adsorbed on the surface in order to maintain the roughening.

The present study demonstrates the change of surface structure of a vicinal surface under low pressure ($1x10^{-3}$ mbar) CO and various dosing conditions. However, in order to fully understand the dynamics of the roughening process, the conditions needed for the roughening and why the (110) facets were not found, further studies are needed.

Chapter 5

Acknowledgement

I would like to express my sincere gratitude to my supervisors, Johan Gustafson and Lindsay Merte, and PhD student Chu Zhang for the continues guidance and support through of my Bachelor diploma work and patiently proof-reading my thesis. I feel very lucky that I can contribute and get involved in the research process with them.

Bibliography

[1] Chu Zhang, Edvin Lundgren, Per-Anders Carlsson, Olivier Balmes, Anders Hellman, Lindsay R Merte, Mikhail Shipilin, Willem Onderwaater, and Johan Gustafson. Faceting of rhodium (553) in realistic reaction mixtures of carbon monoxide and oxygen. *The Journal of Physical Chemistry C*, 2015.

[2] J Gustafson, A Resta, A Mikkelsen, R Westerström, JN Andersen, E Lundgren, J Weissenrieder, M Schmid, P Varga, N Kasper, et al. Oxygen-induced step bunching and faceting of rh (553): Experiment and ab initio calculations. *Physical review B. Condensed matter and materials physics*, 74(3), 2006.

[3] Andreas Stierle and Alfons M Molenbroek. Novel in situ probes for nanocatalysis. *MRS bulletin*, 32(12):1001–1009, 2007.

[4] Rasmus Westerström, Johan Gustafson, Andrea Resta, Anders Mikkelsen, Jesper N Andersen, Edvin Lundgren, N Seriani, F Mittendorfer, Michael Schmid, Jan Klikovits, et al. Oxidation of pd (553): From ultrahigh vacuum to atmospheric pressure. *Physical Review B*, 76(15):155410, 2007.

[5] Johan Gustafson, R Westerstrom, O Balmes, A Resta, R Van Rijn, X Torrelles, CT Herbschleb, JWM Frenken, and Edvin Lundgren. Catalytic activity of the rh surface oxide: Co oxidation over rh (111) under realistic conditions. *The Journal of Physical Chemistry C*, 114(10):4580–4583, 2010.

[6] Hans Lüth. *Solid surfaces, interfaces and thin films*, volume 4. Springer, 2001.

[7] M-C Desjonqueres. *Concepts in Surface Physics: 2ème édition*, volume 30. Springer Science & Business Media, 1996.

[8] B Lang, RW Joyner, and GA Somorjai. Low energy electron diffraction studies of chemisorbed gases on stepped surfaces of platinum. *Surface Science*, 30(2):454–474, 1972.

[9] Gerd Binnig, Heinrich Rohrer, Ch Gerber, and Eddie Weibel. Tunneling through a controllable vacuum gap. *Applied Physics Letters*, 40(2):178–180, 1982.

[10] C Julian Chen. *Introduction to scanning tunneling microscopy*. Oxford University Press, 2008.

[11] Victor Watson Brar. Scanning tunneling spectroscopy of graphene and magnetic nanostructures. 2010.

[12] Ralph Howard Fowler and L Nordheim. Electron emission in intense electric fields. In *Proceedings of the Royal Society of London A: Mathematical, Physical and Engineering Sciences*, volume 119, pages 173–181. The Royal Society, 1928.

[13] S. Woedtke. Ph.d. thesis. 2002.

[14] Michel A Van Hove, William H Weinberg, and Chi-Ming Chan. *Low energy electron diffraction*, volume 20. Springer, Berlin, 1986.

[15] Bipin K Agarwal et al. X-ray spectroscopy. *Springer Series in Optical Sciences*, 15, 1991.

[16] John C Fuggle and John E Inglesfield. Unoccupied electronic states. In *Topics in Applied Physics*, volume 69, pages 1–23.

[17] Feng Tao, Sefa Dag, Lin-Wang Wang, Zhi Liu, Derek R Butcher, Hendrik Bluhm, Miquel Salmeron, and Gabor A Somorjai. Break-up of stepped platinum catalyst surfaces by high co coverage. *Science*, 327(5967):850–853, 2010.

[18] David M Rampulla and Andrew J Gellman. Enantioselectivity on surfaces with chiral nanostructures. 2004.